REGULAR ARTICLE

blood advances

p16INK4A-dependent senescence in the bone marrow niche drives age-related metabolic changes of hematopoietic progenitors

Charlotte Hellmich,[1,2] Edyta Wojtowicz,[1,3] Jamie A. Moore,[1] Jayna J. Mistry,[1,3] Aisha Jibril,[1] Benjamin B. Johnson,[1] James G. W. Smith,[1] Naiara Beraza,[4] Kristian M. Bowles,[1,2] and Stuart A. Rushworth[1]

[1]Norwich Medical School, University of East Anglia, Norwich Research Park, Norwich, United Kingdom; [2]Department of Haematology, Norfolk and Norwich University Hospitals NHS Trust, Norwich, United Kingdom; [3]Earlham Institute, Norwich Research Park, Norwich, United Kingdom; and [4]Gut Microbes and Health Institute Strategic Programme, Quadram Institute, Norwich, United Kingdom

Key Points

- Accumulation of senescent MSCs in the aging BM impairs their ability to support hematopoietic stem cells in response to stress.
- Rejuvenation of the aged BM niche allows aged HPCs to recover their metabolic response to stress.

Rapid and effective leukocyte response to infection is a fundamental function of the bone marrow (BM). However, with increasing age, this response becomes impaired, resulting in an increased burden of infectious diseases. Here, we investigate how aging changes the metabolism and function of hematopoietic progenitor cells (HPCs) and the impact of the BM niche on this phenotype. We found that, in response to lipopolysaccharide-induced stress, HPC mitochondrial function is impaired, and there is a failure to upregulate the TCA cycle in progenitor populations in aged animals compared with young animals. Furthermore, aged mesenchymal stromal cells (MSCs) of the BM niche, but not HPCs, exhibit a senescent phenotype, and selective depletion of senescent cells from the BM niche, as well as treatment with the senolytic drug ABT-263, improves mitochondrial function of HPCs when stressed with lipopolysaccharide. In summary, age-related HPC metabolic dysfunction occurs indirectly as a "bystander phenomenon" in the aging BM niche and can be restored by targeting senescent MSCs.

Introduction

As our population ages, the burden of age-related diseases increases, and the need to better understand the physiological changes that occur with aging has become apparent.[1] The increased susceptibility to infection, coupled with a reduced ability to effectively clear infections, is just one example of how aging affects disease development.[1] Key to the body's response to infection is the immune system and the ability of the bone marrow (BM) to respond rapidly and effectively to stress stimuli.[2] However, a number of changes have been described as occurring in the aged BM, including reduced ability for self-renewal and long-term repopulation of hematopoietic stem cells (HSCs), myeloid skewing, and upregulation of genes associated with inflammation and stress responses.[3-5] This affects overall BM function and in particular the ability of HSCs and hematopoietic progenitor cells (HPCs) to respond to stressors such as infection or acute hemorrhage.

The energy requirements of HSCs can vary significantly, and mechanisms to allow rapid changes in energy production are vital to permit rapid expansion of the HSC and downstream progenitor populations in response to stress.[6,7] Although quiescent HSCs primarily rely on glycolysis in their hypoxic BM niche, they

Submitted 11 January 2022; accepted 21 May 2022; prepublished online on *Blood Advances* First Edition 27 May 2022; final version published online 17 January 2023. https://doi.org/10.1182/bloodadvances.2022007033.

All relevant data are included in the manuscript and the supporting information files. The data generated in this study are provided upon request from the corresponding authors, Stuart A. Rushworth (s.rushworth@uea.ac.uk) and Kristian M. Bowles (k.bowles@uea.ac.uk).

The full-text version of this article contains a data supplement.

are able to rapidly switch to oxidative phosphorylation (OXPHOS) in response to various stressors.[8] This switch is facilitated by the transfer of mitochondria from mesenchymal stromal cells (MSCs) to the HSCs and supports rapid HSC expansion and emergency granulopoiesis.[9] This action shows that mitochondrial function and health are important in normal HSC function.

Mitochondrial health is known to decline with age,[10] and mitochondrial dysfunction has been associated with a decline in tissue function and a senescent phenotype in a number of different cell populations.[11-13] The hallmark of cellular senescence is the irreversible arrest of cell proliferation,[14] regulated by the p53/p21 and $p16^{INK4a}$/pRB pathways.[15] Senescent cells are known to accumulate in tissues with age,[16] where they have been shown to disrupt tissue function and contribute to the development of age-related diseases,[17-21] including hematologic malignancies.[17] Although this shows that senescent changes can occur in the BM niche in the context of disease, the changes that occur within the BM with aging remain to be explored.

The current study examines how aging in the BM niche changes the metabolic response of HPCs to stress, using lipopolysaccharide (LPS) treatment as a mimic of infection. We determined the changes in mitochondrial function in both HPCs and MSCs and how these affect the ability of HPCs to rely on oxidative phosphorylation. We also studied the role of senescence in the BM niche and how the elimination of senescent cells alters HPC mitochondrial function in response to stress. We explored the role of ABT-263 as senolytic in this setting, thus suggesting that targeting senescence in the BM niche may present potential future therapeutic targets.

Experimental procedures

Animals

C57BL/6J mice (CD45.2) and CBA mice were purchased from Charles River Laboratories (Edinburgh, UK). B6.SJL-$Ptprca^{Pep3b/BoyJ}$ (CD45.1) (PepCboy) and p16-tdTom mice were purchased from The Jackson Laboratory (Bar Harbor, ME). p16-3MR mice were developed and provided by the Campisi laboratory.[16] This is a mouse model with a 3 modality reporter gene associated with the p16 promotor. The component of the model used for this study is the herpes simplex virus 1 thymidine kinase reporter, which phosphorylates the pro-drug ganciclovir (GCV) and converts it to a DNA chain terminator, causing apoptosis of senescent cells.

All mice were housed in a specific pathogen-free facility, and all animal work was conducted in accordance with regulations set by the UK Home Office and the Animal Scientific Procedures Act 1986. Female mice were used for all experiments. Animals were aged 18 to 24 months; the young mice used were 8 to 12 weeks old.

In vivo treatments

LPS was administered by intraperitoneal injection at a dose of 0.5 mg/kg, and animals were killed 16 hours after this treatment. GCV was administered by intraperitoneal injection at a dose of 25 mg/kg for 5 days to aged p16-3MR mice and control C57Bl/6 mice. ABT-263 was administered by oral gavage at a dose of 100 mg/kg daily for 7 days.

Cell isolation and preparation

BM was isolated from the tibias and femurs of each mouse by cutting the bone in half and placing it in a 0.5 mL Eppendorf tube with a hole at the base; this was then placed in an intact 1.5 mL Eppendorf tube and centrifuged on full power for 6 seconds to collect the cells from each bone. The cell pellets were pooled for each mouse, filtered, and then washed with MACS buffer (1X phosphate buffer solution, pH 7.4 containing 0.5% bovine serum albumin and 1 mM EDTA). Cells were then counted if needed and prepared for flow cytometry, fluorescent-activated cell-sorting (FACS), or in vitro use.

BM transplantation

For the transplantation model, aged CD45.2-expressing C57Bl/6 mice were used, their BM was isolated as described in the prior paragraph, and LSK (Lin^-, $Sca1^+$, $c\text{-}Kit^+$) cells were separated by FACS. These cells were then injected into young CD45.1 expression PepCboy mice by tail vein injection at a concentration of 2×10^4 cells in 200 µL. Before transplant, young C57Bl/6 mice were primed with 3 days of busulfan treatment, 25 mg/kg intraperitoneally. Engraftment was confirmed by peripheral blood (PB) sampling at 8 and 12 weeks.

Flow cytometry and cell sorting

For experiments with MitoTracker Green (MTG; Thermo Fisher Scientific, Waltham, MA) or tetramethylrhodamine, methyl ester (TMRM; Thermo Fisher Scientific), cells were first incubated with 200 nM MTG (I Thermo Fisher Scientific) together with 50 µM verapamil (MilliporeSigma, Burlington, MA), 400 nM TMRM for 30 minutes at room temperature. They were then washed twice with MACS buffer and centrifuged at 1500 rpm for 5 minutes before staining with antibodies. Antibody cocktails were prepared in MACS and incubated with BM cells for at least 30 minutes at 4°C. The following antibodies were used: lineage (Lin)-negative cocktail-pacific blue (Miltenyi Biotec, Bergisch Gladbach, Germany), Sca1-APC (Miltenyi Biotec), CD117-PE Vio770 (Miltenyi Biotec), CD48-APC-Cy7 (BioLegend, San Diego, CA), CD150-BV510 (BioLegend), CD117-FITC (BioLegend), BCL-2-PE Vio770 (Miltenyi Biotec), BCL-XL-FITC (Cell Signaling Technology, Danvers, MA), CD45-BV510 (BioLegend), CD45-PerCP (BioLegend), CD31-FITC (Miltenyi Biotec), CD31-PeCy5 (BioLegend), Ter119-APC Biolegend), CD105-PE Vio770 (Miltenyi Biotec), CD105-FITC (Miltenyi Biotec), CD140a-APC-Cy7 (BioLegend), CD45.1-PE (Miltenyi Biotec), CD45.1-APC (Miltenyi Biotec), CD45.2-FITC (Miltenyi Biotec), Gr1-PerCP (Miltenyi Biotec), Cd11b-PeCy5 (BioLegend), CD3-PE (BioLegend), and B220-PE (BioLegend). Compensations and fluorescence minus one controls were run before each experiment. A total of 100 000 gated events where recorded for each BM sample.

For FACS, the BM cells were re-suspended in MACS buffer and stained with antibody mix; cells were sorted into MACS buffer for transplants or directly into RNA lysis buffer. A FACSCanto II flow cytometer (BD Biosciences, Franklin Lakes, NJ) was used for all flow cytometry, and cell sorting was conducted on a BD FACS-Melody (BD Biosciences). Data were analyzed by using FlowJo version 10.8.1 (Becton, Dickinson and Company, Ashland, OR). Specific gating strategies are provided in the figures.

Cell culture

LK (Lin^-, $c\text{-}Kit^+$) cells were isolated by using direct lineage depletion, and $CD117^+$ enrichment kits (Miltenyi Biotec) were used. The resulting LK cells were cultured in Dulbecco's modified Eagle medium containing 10% fetal bovine serum and 1% penicillin-streptomycin, supplemented with murine stem cell factor

(100 ng/mL), murine interleukin-3 (IL-3) (10 ng/mL), and human IL-6 (100 ng/mL) (PeproTech, Rocky Hill, NJ) or used immediately for Seahorse metabolic flux analysis. MSCs were isolated from whole BM by adherence to tissue culture plastic. MSCs were then expanded in minimum essential media containing 20% fetal bovine serum plus 1% penicillin-streptomycin. MSC markers were confirmed by flow cytometry ($CD105^+$, $CD140a^+$ $CD31^-$, $Ter119^-$, $CD45^-$).

Senescence β-galactosidase assay

Senescence β-galactosidase staining kit (Cell Signaling Technology) was used to detect senescence-associated β-galactosidase in isolated LK cells from young and aged mice. LK cells were cultured and treated in 35-mm dishes. The LK cells were evaluated for the blue color, indicative of cells positive for senescence-associated β-galactosidase.

Seahorse

XFp flux cartridges were hydrated in XF Calibrant (Agilent Technologies, Santa Clara, CA) overnight at 37°C. LK cells were resuspended in Seahorse base media supplemented with pyruvate (1 mM), L-glutamine (2 mM), and glucose (10 mM). A total of 100 000 cells were plated onto each well of a Seahorse XFp culture plate coated with poly-D-lysine and centrifuged briefly to achieve a uniform monolayer of cells. Cells were equilibrated in a humidified non–carbon dioxide incubator until the start of the assay. Flux cartridges were loaded with oligomycin (2 μM), carbonyl cyanide-4-(trifluoromethoxy) phenylhydrazone (1 μM), and rotenone (0.5 μM) according to manufacturer's instructions. Oxygen consumption rate (OCR) and basal extracellular acidification rate values were obtained by using the Agilent Seahorse XFp Mito Stress Kit. OCR is known to reflect levels of OXPHOS within the cells, whereas the extracellular acidification rate is a measure of glycolysis. All results were normalized to input cell number.

Metabolic pathway analysis

MitoPlates were prepared following manufacturer's instructions; 30 μL assay mix containing 50 μg/mL saponin (47036-50G-F; MilliporeSigma) was pipetted into the wells and incubated at 37°C for 1 hour. During this incubation, $CD117^+$ cells were harvested as described earlier, filtered by using a 40 μm nylon filter, and counted. Cells were pelleted, resuspended in 1x MAS Buffer (72303; Biolog, Inc., Hayward, CA), creating a final concentration of 2.5×10^6 cells/mL; 30 μL of cell resuspension was then pipetted into each well of the MitoPlate (14105; Biolog, Inc.). The MitoPlate was read for 6 hours with 5-minute intervals at an optical density (OD) of 590 nm using the OmniLog plate reader. The initial and final OD readings were separated and organized per well. Data were restructured to fit correct MitoPlate format, the final OD reading was subtracted against the initial OD, and any negative results were set to 0. The triplicate no-substrate control wells were averaged; each individual calculated OD value was subtracted from this value and averaged, creating the average aggregate minus no substrate table. The negatives were removed from this table and the data reorganized to match each substrate. To create the heatmaps, final data were normalized to young control and highlighted using 3-color conditional formatting.

Real-time quantitative polymerase chain reaction

RNA was isolated by using the ReliaPrep RNA Cell Miniprep System (Promega, Southampton, UK). Nugen PicoSL WTA (Tecan Genomics, Redwood City, CA) was used to generate first-strand and double-strand complementary DNA, followed by complementary DNA amplification. Quantitative reverse transcription polymerase chain reaction (qRT-PCR) assay was performed with SYBR Green technology (PCR Biosystems, London, UK). PCRs were amplified for 45 cycles (95°C/15 seconds, 60°C/10 seconds, and 72°C/10 seconds), after pre-amplification (95°C/60 seconds), on a 384-well/96-well LightCycler480 (Roche Life Science, Indianapolis, IN). Messenger RNA expression was normalized against glyceraldehyde-3-phosphate dehydrogenase using the comparative cycle threshold method.

For the coculture experiment assessing mitochondrial content and to quantify mitochondrial DNA content in cell populations, DNA was extracted by using the PureLink Genomic DNA Mini kit (Thermo Fisher Scientific). qRT-PCR using TaqMan probes ND3 and COX3 (Thermo Fisher Scientific) was then performed. ND3 and COX3 TaqMan assays were run in simplex reactions. After pre-amplification (60°C for 30 seconds and 95°C for 5 minutes), the PCRs were amplified for 50 cycles (95°C for 15 seconds and 60°C for 1 minute) and cooled (40°C for 30 seconds) on a 384-well LightCycler 480 (Roche, Burgess Hill, UK). Each mitochondrial DNA level was normalized against the genomic DNA.

Quantification and statistical analysis

Statistical analysis was performed by using Prism version 9.10 (GraphPad Software, La Jolla, CA). Due to variability in the data, statistical comparison of in vivo work was performed without assumption of normal distribution by using a Mann-Whitney test. Differences among groups were considered significant as follows: $*P < .05$, $**P < .01$, and $***P < .001$. Sample size (n) represents number of biological replicates. No statistical methods were used to predetermine sample size. For statistical comparison of >2 groups, the two-way analysis of variance was performed.

Results

Hematopoietic progenitors from aged mice show an impaired metabolic response to LPS treatment

Mitochondrial health has been shown to decrease with age.[10] To determine how this affects the ability of HPCs to respond to stress, both young (8-12 weeks old) and aged (18-24 months old) mice were treated with LPS; after 16 hours, their BM was isolated (Figure 1A). The total BM cellularity was found to be increased in aged mice, which is consistent with previously published data (supplemental Figure 1A).[22,23] Cell counts of HPC populations, including LSKs (Lin^-, $Sca1^+$, $c\text{-}Kit^+$), LS-Ks (Lin^-, $Sca1^-$, $c\text{-}Kit^+$), and multipotent progenitors (MPPs) (Lin^-, $Sca1^+$, $c\text{-}Kit^+$, $CD150^-$, $CD48^+$) were determined for both young and aged mice after LPS treatment compared with control mice (Figure 1B-C). In young mice, there was a significant expansion of LSKs and MPPs after LPS treatment, although no change in LS-K counts was observed. However, in aged mice, this increase was not observed in any of the cell populations. To assess the metabolic changes after LPS treatment, mitochondrial membrane potential ($\Delta\Psi m$) and mitochondrial content were measured by using TMRM (a dye that accumulates in mitochondria with intact membrane potential) and MTG, respectively. As previously described,[24] 2 distinct cell populations, TMRM high ($TMRM^{hi}$) and TMRM low, were identified in both aged and young HPCs (Figure 1D). The frequency of $TMRM^{hi}$

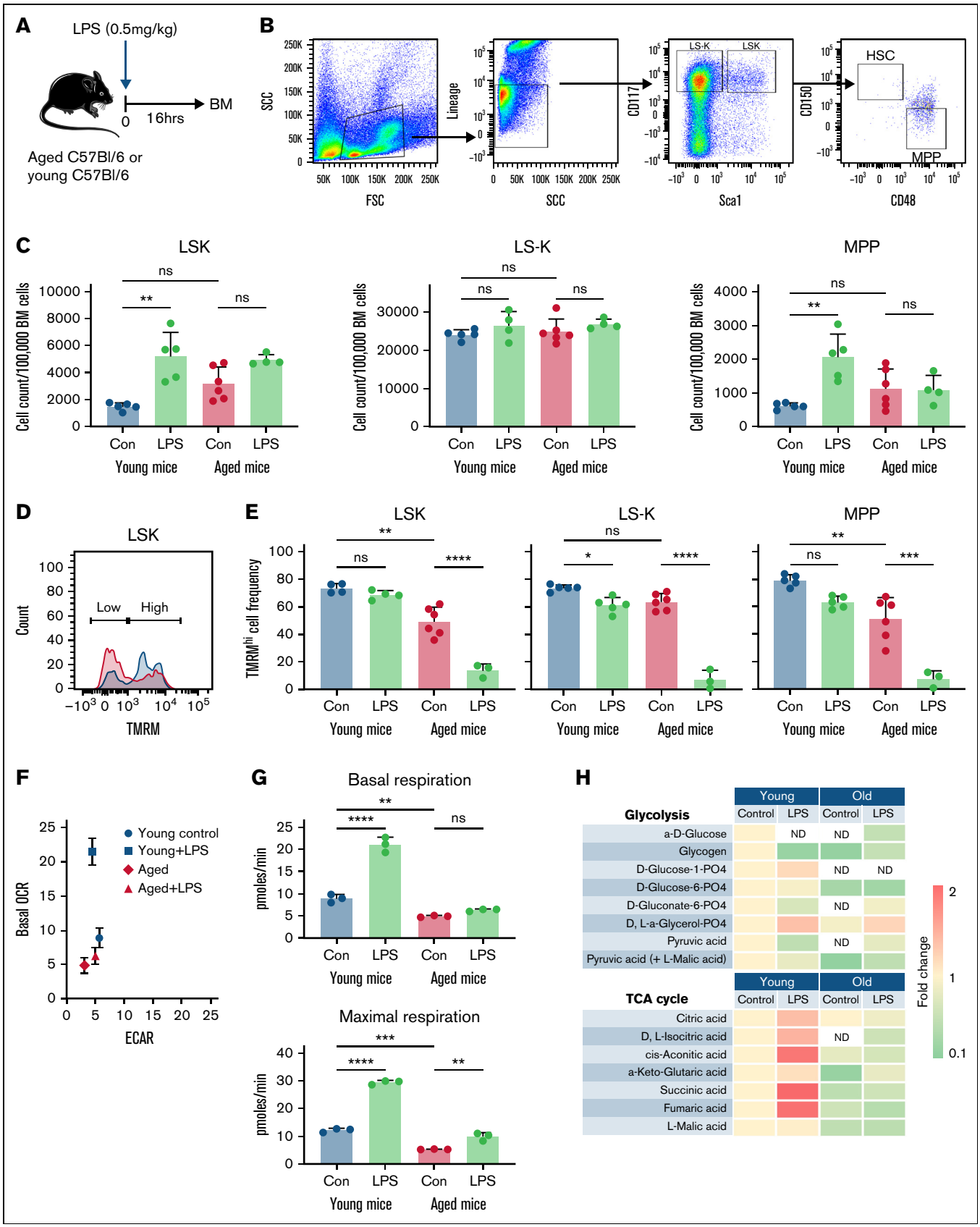

Figure 1.

LSKs and MPPs was reduced in aged mice compared with young mice, and there was no change in the TMRM^{hi} frequency in the LS-K population (Figure 1E). After LPS treatment, the frequency of TMRM^{hi} LSKs, LS-K, and MPPs was found to be reduced both in young and in aged mice, probably due to the increased metabolic demand causing increased intracellular stress.

TMRM is a measure of $\Delta\Psi$m but not OXPHOS. We therefore next examined the entire LK (Lin$^-$, c-Kit$^+$) population for metabolic output using the Seahorse metabolic flux assay and rates of substrate metabolism using MitoPlates from Biolog, Inc. Cells from aged mice did not shift toward OXPHOS, as measured by OCR, in response to LPS compared with LKs from young mice (Figure 1F-G). Furthermore, metabolic substrate analysis showed that LKs from young mice increased the metabolism of mitochondrial TCA cycle substrates in response to LPS-induced stress (Figure 1H), and this action was not observed in aged LKs. This suggests that mitochondrial output of HPC in aged mice is impaired under stressed conditions.

Transplantation of aged LSKs into young mice reverses the aged HPC mitochondrial phenotype

The BM niche is known to be crucial for HSC and HPC function. To determine if the changes observed in aged HPCs under stress are driven by the niche or occur as a consequence of HPC aging, we FACS-purified and adoptively transferred young or old LSKs from C57Bl/6 mice (CD45.2$^+$) into young PepCboy (CD45.1$^+$) mice (Figure 2A). After 12 weeks, mice were killed and engraftment was confirmed by measuring the distribution of CD45.1$^+$ and CD45.2$^+$ cells in the LSK, LS-K, and MPP compartment and in the PB. A slightly higher engraftment of young progenitor cells compared with the old was observed (Figure 2B). However, this finding did not result in differences in the lymphoid/myeloid ratio of the mature PB cells after transplantation (Figure 2C). Furthermore, donor CD45.2$^+$ LSK numbers and TMRM^{hi} frequencies of all donor CD45.2$^+$ progenitor cells were similar in mice transplanted with aged or young LSKs (Figure 2D-E).

Next, recipients transplanted with LSKs from aged mice were treated with LPS (Figure 2F). The data show that transplanting aged LSKs into young mice results in LSK expansion, similarly to that observed in mice transplanted with young LSKs (Figure 2G). Furthermore, analysis of $\Delta\Psi$m in HPCs revealed that TMRM^{hi} frequency was unchanged in LSKs, LS-Ks, and MPPs after LPS treatment of mice transplanted with LSKs from aged mice (Figure 2H). This finding suggests an improved metabolic response to LPS treatment compared with that in aged mice, in which TMRM^{hi} HPC frequencies were reduced after LPS treatment (Figure 1E). To confirm this theory, OCR was measured in aged LKs after transplantation into young mice in response to LPS (Figure 2I-J). OCR increased after LPS treatment in mice transplanted with aged LSKs, and changes were similar to those observed in mice transplanted with young LSKs. Together, these data suggest that the niche in which HPCs reside is essential for their maintenance and health and allows for a strong metabolic response to stress.

Aged MSCs accumulate mitochondria with low membrane potential resulting in a senescent phenotype

To characterize the age-related changes within the BM niche, MSCs, defined as CD45$^-$, Ter119$^-$, CD31$^-$, and CD105$^+$ cells (Figure 3A),[25,26] were first analyzed for cell numbers and $\Delta\Psi$m and mitochondrial content. In the aged BM, there was an increase in MSC numbers (Figure 3B), and the frequency of TMRM^{hi} MSCs was lower (Figure 3C), although there was no difference in mitochondrial content (Figure 3D) compared with MSCs from young mice. Because mitochondrial dysfunction has previously been associated with aging and has been described as a trigger for cellular senescence,[10,11] we next investigated if p16^{INK4a} or p21 was upregulated in FACS-purified MSCs. We found a significant increase in p16^{INK4a} expression in MSCs from aged mice compared with young mice but no change in p21 expression (Figure 3E). To confirm the upregulation of p16^{INK4a} in MSCs from aged mice, the p16-tdTom mouse model in which p16^{INK4a} promotor is linked to the Ultrabright Fluorochrome Tandem Dimer Tomato (tdTom) was used (Figure 3F). Increased fluorescence was detected in aged MSCs compared with young (Figure 3G). Furthermore, MSCs from aged mice were found to have an increase in the senescence-associated secretory phenotype component IL-6 expression (Figure 3H) and a decrease in laminin B1 expression (Figure 3I); both of these are characteristic features of senescent cells. Conversely, the LSK population had no change in p16^{INK4a} expression (Figure 3J), and detection levels of p16^{INK4a}-driven tdTom fluorescence were very low (supplemental Figure 3A). There was also no change in β-galactosidase staining in the LSKs (supplemental Figure 3B). Interestingly, p21 expression was in fact reduced in the LSKs from aged mice compared with young mice. Together, these data suggest that MSCs, but not HPCs, within the BM acquire a senescent phenotype with aging.

Our group has previously shown that mitochondrial transfer occurs between MSCs and HSCs in response to stress.[8] We therefore investigated whether this mechanism is altered in the aged BM. However, the results show that aged MSCs continue to be able to transfer mitochondria to HPCs in response to stress (supplemental Figure 3C-E) and that even though mitochondrial content is reduced after LPS treatment in MSCs from both young and aged mice, their $\Delta\Psi$m remains stable (supplemental Figure 3C,F).

Figure 1. Hematopoietic progenitors from aged mice exhibit an impaired metabolic response to LPS treatment. (A) Schematic of the experiment. Young (8-12 weeks) and aged (18-24 months) C57Bl/6 mice were treated with 0.5 mg/kg LPS or vehicle control. After 16 hours, they were killed and their BM isolated. (B) Flow cytometry gating strategy and for LSK, LS-K, MPP, and HSC (Lin$^-$, Sca1$^+$, cKit$^+$, CD150$^+$, CD48$^-$) populations in aged mice. (C) LSK, LS-K, and MPP cell counts per 100 000 BM cells in young and aged mice after LPS treatment compared with control mice. (D) Example of TMRM^{hi} and low cell populations in young (blue) and aged (red) mice and frequencies of TMRM^{hi} LSKs. (E) Frequencies of TMRM^{hi} LSKs, LS-Ks, and MPPs after LPS treatment in young and aged mice. (F) Changes in OCR compared with extracellular acidification rate (ECAR) in LKs isolated from aged and young mice after LPS treatment. (G) Changes in basal and maximal respiration after LPS treatment in LKs from young and aged mice. (H) Results from the Biolog analysis showing the metabolic utilization of glycolytic and TCA cycle substrates by LKs isolated from young and aged mice treated with LPS compared with control mice. Not detected (ND) levels are labeled, and 1 represents no change. *$P < .05$, **$P < .01$, ***$P < .001$, ****$P < .0001$ using the Mann-Whitney U test or two-way analysis of variance. Con, vehicle control; FSC, forward scatter; SCC, side scatter; ns, not significant.

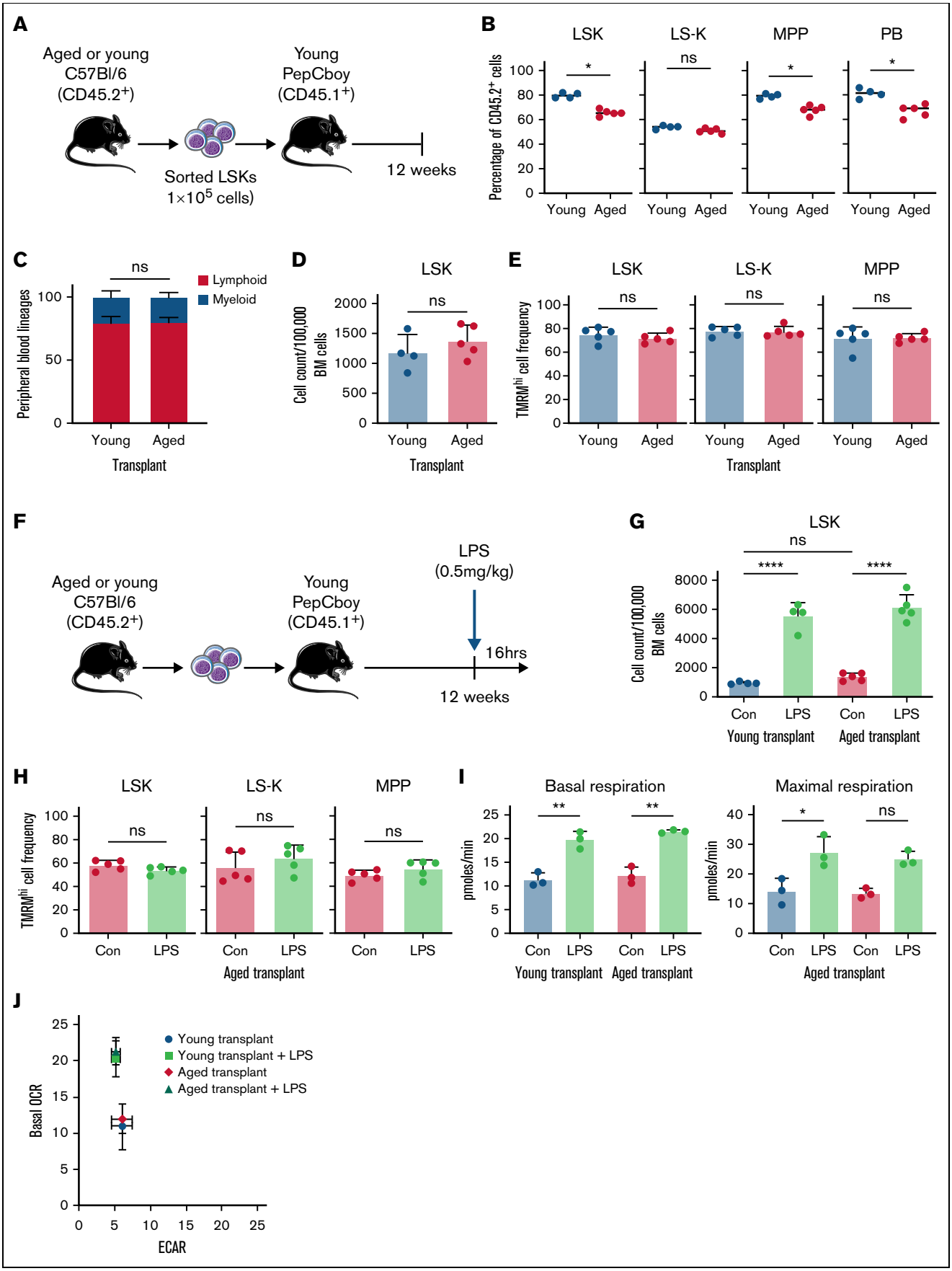

Figure 2.

Selective depletion of senescent MSC in the BM niche allows recovery of HPC mitochondrial health in aged mice

It is likely that the pathways which contribute to cellular senescence during natural aging are activated by a number of factors, including DNA damage, telomere shortening, oncogenic activation, and mitochondrial dysfunction.[27,28] Thus, although mitochondrial dysfunction may not be the driver of MSC senescence, the acquisition of a senescent phenotype could be detrimental to their ability to support HPC expansion in response to stress. In the p16-3MR mouse model, GCV selectively depletes senescent cells.[16] Treatment of aged p16-3MR mice with GCV (Figure 4A) resulted in a decrease in MSC numbers in the BM compared with aged C57Bl/6 mice treated with GCV (Figure 4B). MSCs from p16-3MR mice treated with GCV were found to have a stable frequency of TMRM^{hi} MSCs compared with aged C57Bl/6 control mice (Figure 4C). This finding suggests that GCV treatment selectively depletes senescent MSCs but has no direct impact on the $\Delta\Psi$m of the MSCs in aged mice. No significant change was observed in the counts or TMRM levels of HPCs after LPS treatment in aged p16-3MR mice previously treated with GCV (Figure 4D-E). This suggests that although the cell expansion was not significant, as is seen in young mice (Figure 1C), the $\Delta\Psi$m appears to be more stable in p16-3MR mice treated with GCV followed by LPS, and there is no significant drop in TMRM^{hi} cell frequency, as is observed in aged mice (Figure 1E). Moreover, Seahorse metabolic flux analysis of LSKs displayed an increase in basal and maximal OCR (Figures 4F-G). C57Bl/6 mice treated with GCV and LPS were used as controls. Because treatment with GCV resulted in no change in the $\Delta\Psi$m of MSCs, our data suggest that it is the senescent phenotype of the MSC rather than the direct effect of the MSC mitochondrial function that alters the response of aged HPCs to stress. Here, we show that depletion of these senescent cells in aged mice allows for a shift in the metabolic output of aged HPCs in response to LPS.

Others have reported that the drug ABT-263, which targets the antiapoptotic proteins BCL-2, BCL-XL, and BCL-W, acts as an effective senolytic and treatment for total body irradiated animals, with ABT-263 reversing the onset of premature aging of the hematopoietic system.[5] We therefore hypothesized that ABT-263 would selectively target the senescent MSCs within the aged BM niche and that this in turn would help to improve the metabolic response of HPCs to stress. Aged mice were treated with ABT-263 or vehicle control daily for 7 days, and MSCs were shown to be reduced after ABT-263 treatment (Figure 5A). Moreover, sorted MSCs had lower levels of p16^{INK4a} expression than those of ABT-263–treated animals (Figure 5B). It would also be of interest to determine if ABT-263 treatment directly affects the $\Delta\Psi$m of MSCs, or whether, as described earlier, the changes observed are primarily driven through targeting of the senescent phenotype. HPC expansion after LPS treatment was restored in mice first treated with ABT-263 (Figure 5C). Furthermore, mice treated with ABT-263 had a stable TMRM^{hi} LSK and MPP frequency after LPS treatment, whereas the frequency of TMRM^{hi} LS-K was slightly reduced in a pattern similar to that observed in young mice (Figure 5D). The HPC populations displayed no difference in TMRM^{hi} frequency after LPS treatment, and Seahorse metabolic flux analysis showed that ABT-263 improved the OCR of the downstream progenitor population in response to LPS treatment (Figure 5E). Moreover, metabolic pathway analysis revealed that ABT263 treatment enhanced the utilization of TCA cycle substrates, and this was further increased in response to LPS (Figure 5F). Together, our data show that in the aging BM, it is the MSCs, not the HPCs, that are senescent, and targeting these for deletion improves HPC metabolism and subsequent expansion in response to stress.

Discussion

The current study found that age-related changes in the BM niche result in an impaired response of HPCs to infection, using LPS as a mimic. This is driven by a senescent phenotype of the MSCs within the BM niche and subsequent accumulation of dysfunctional mitochondria in MSCs and HPCs. Previous work has shown that transfer of mitochondria and a rapid switch to OXPHOS from glycolysis is required for the HPC response to infection and initiation of emergency granulopoiesis.[8] Our data show that, in the aged BM, the shift toward OXPHOS is impaired in response to stress. Because mitochondrial function is impaired in both MSCs and HPCs in aged mice, this may not be due to a fault in the mechanism of transfer but rather result from the transfer of dysfunctional mitochondria from the MSCs to HPCs. Thus, HPCs in aged mice are unable to adequately increase OXPHOS, not because of an intrinsic cellular defect but as a consequence of the aged niche in which they reside. Further studies would be needed to define the role of the various BM cell populations in this interaction. In addition, age-related changes in HSC function and their response to stress remain to be explored. Due to small numbers and sensitivity of HSCs, many of the metabolic assays are difficult to perform in HSCs; however, defining BM senescence-driven changes in the HSC population of aged mice would add further value to the findings described here.

Figure 2. Transplantation of aged LSKs into young mice reverses the aged HPC mitochondrial phenotype. (A) Schematic of the experiment for the adoptive transfer of young and aged LSKs into young mice. BM was isolated from young and aged C57Bl/6 mice (CD45.2$^+$), and LSKs were separated by FACS. They were transplanted into young PepCboy mice (CD45.1$^+$). At 12 weeks, mice were killed, their BM was isolated, and terminal blood samples were taken. Flow cytometry was used to assess the engraftment. (B) Percentage of CD45.2$^+$ engrafted LSKs, LS-Ks, MPPs, and PB cells in mice transplanted with LSKs from either young or aged mice. (C) Analysis of PB lineages was performed to evaluate the proportion of lymphoid (CD3$^+$ B220$^+$) and myeloid (Gr1$^+$ CD11b$^+$) cells in mice transplanted with LSKs from young or aged mice. (D) CD45.2$^+$ LSK cell counts per 100 000 BM cells in mice transplanted with LSKs from young or aged mice. (E) Frequency of CD45.2$^+$ TMRM^{hi} LSKs, LS-Ks, and MPPs isolated from mice 12 weeks after transplant with young or aged LSKs. (F) Schematic of the experiment. After engraftment of LSKs from aged C57Bl/6 mice was confirmed in the young PepCboy recipients at 12 weeks, the transplanted PepCboy mice were treated with 0.5 mg/kg LPS or vehicle control. After 16 hours, their BM was isolated, and analysis was conducted on CD45.2$^+$ engrafted cells. (G) Number of LSKs in mice transplanted with aged LSKs and then treated with LPS or vehicle control. (H) Frequency of TMRM^{hi} LSKs, LS-Ks, and MPPs from control and LPS-treated mice. (I) Basal and maximal respiration of LKs after LPS treatment compared with controls, measured by Seahorse metabolix flux analysis. (J) Changes in OCR compared with extracellular acidification rate (ECAR) in control and LPS-treated mice previously transplanted with LSKs from aged mice. *$P < .05$, **$P < .01$, ****$P < .0001$ using the Mann-Whitney U test or two-way analysis of variance. Con, vehicle control; ns, not significant.

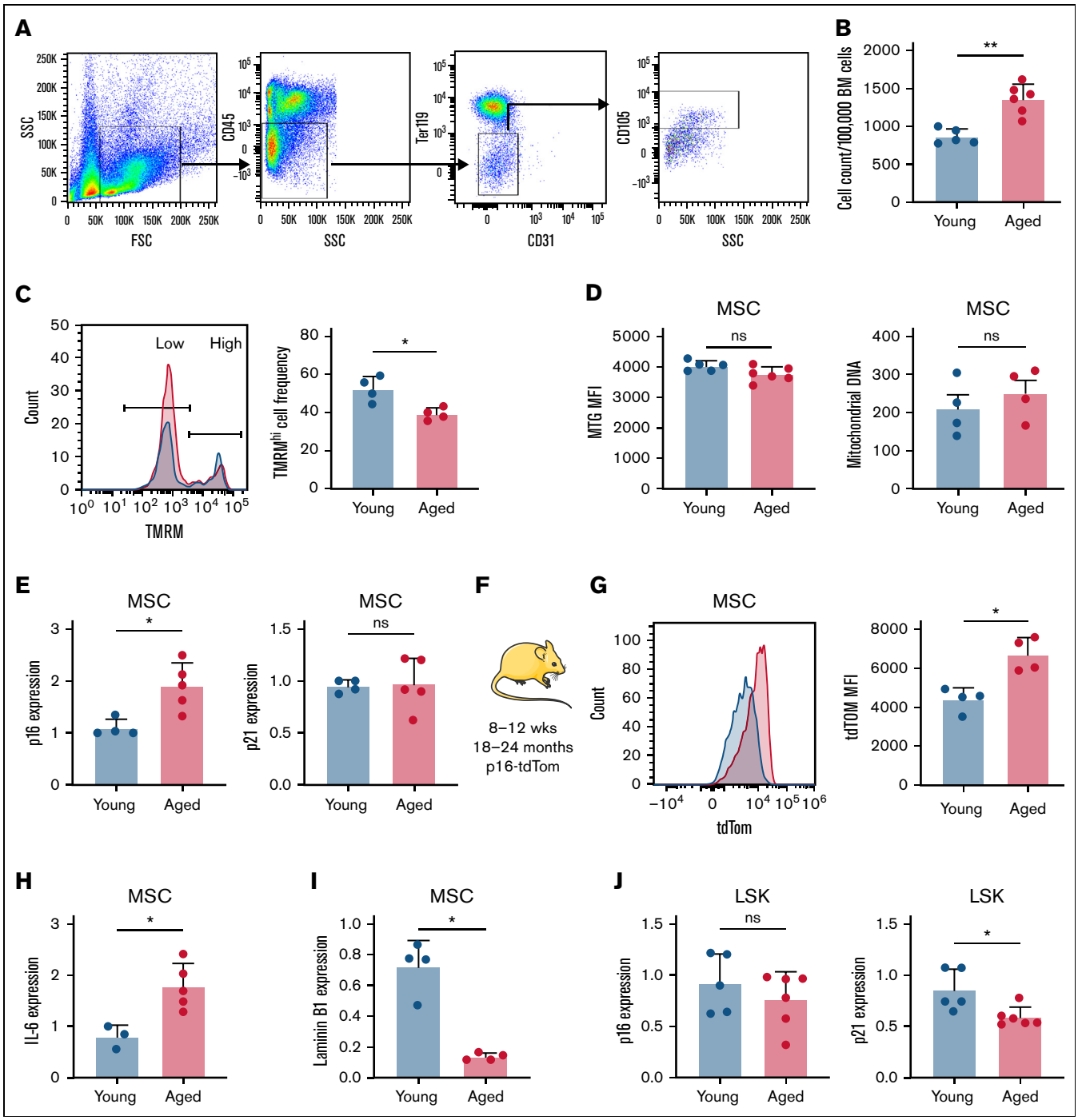

Figure 3. Aged MSCs accumulate mitochondria with low membrane potential, resulting in a senescent phenotype. BM was isolated from young and aged C57Bl/6 mice. (A) Gating strategy for MSCs. (B) MSC counts per 100 000 BM cells from young and aged mice. (C) Representative flow plot of $TMRM^{hi}$ and TMRM low MSC populations in young (blue) and aged (red) mice and comparison of $TMRM^{hi}$ MSC frequency. (D) Mean fluorescent index (MFI) of MTG in MSCs from young and aged C57Bl/6 mice was measured by using flow cytometry, and mitochondrial DNA content was measured relative to genomic DNA by using TaqMan PCR. (E) MSCs were separated by FACS, and gene expression of p16 and p21 was measured by RT-qPCR; expression relative to glyceraldehyde-3-phosphate dehydrogenase (GAPDH) is shown. (F) Schematic of p16-tdTom mouse model in which $p16^{INK4a}$ promotor is linked to tdTom, allowing detection of cells expressing p16 by flow cytometry. (G) Representative flow plot of tdTom expression in young and aged mice and comparison of MFI. (H) Gene expression of IL-6, relative to GAPDH, in MSCs from young and aged mice separated by FACS. (I) Gene expression of laminin B1, relative to GAPDH, in MSCs from young and aged mice separated by FACS. (J) Gene expression of p16 and p21, relative to GAPDH, in LSKs separated by FACS. $^*P < .05$, $^{**}P < .01$ using the Mann-Whitney *U* test or two-way analysis of variance. FSC, forward scatter; ns, not significant; SSC, side scatter.

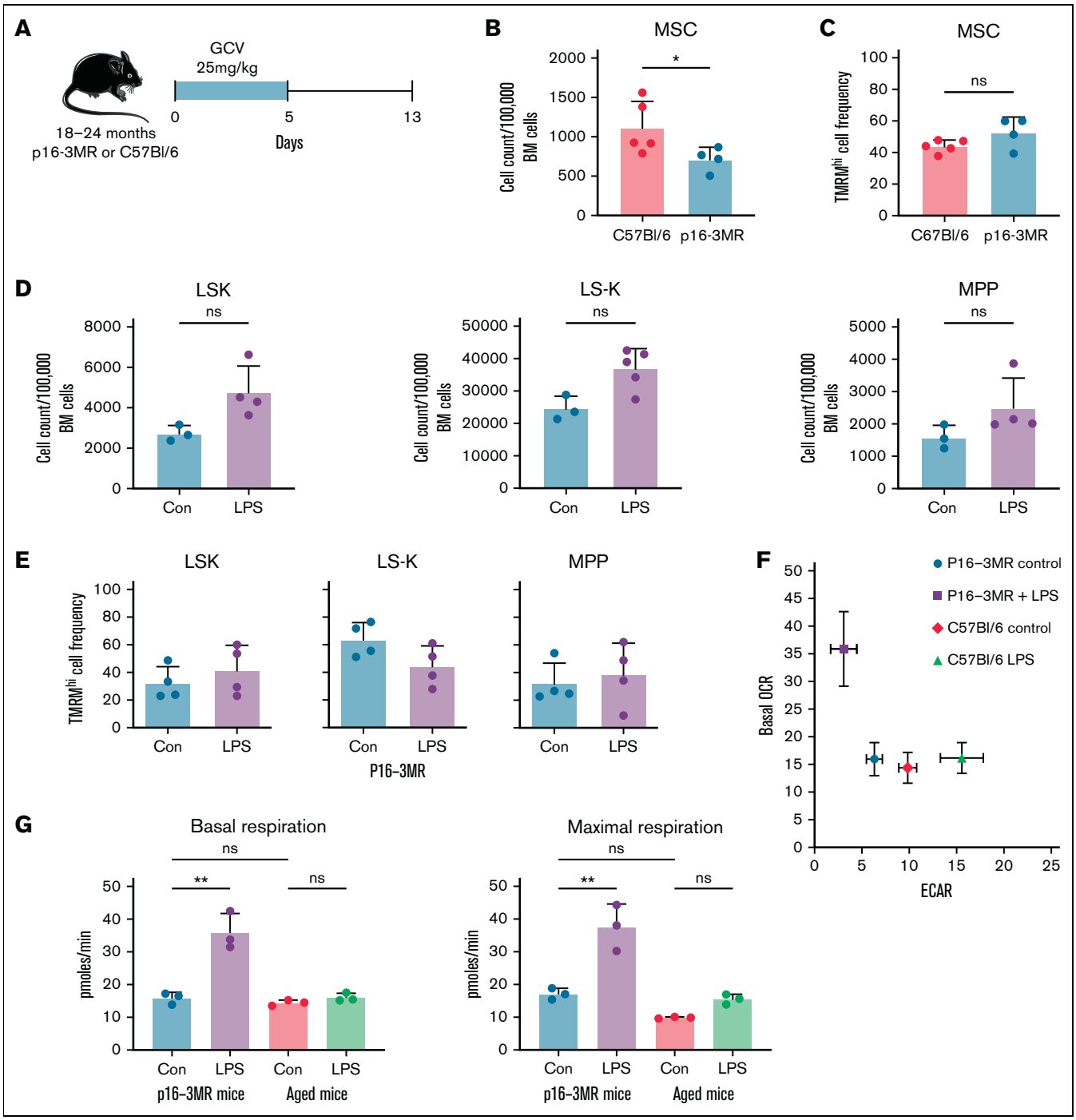

Figure 4. Selective depletion of senescent cells in the BM niche. (A) Schematic of the experiment. Aged p16-3MR mice and C57Bl/6 mice were treated with 25 mg/kg of GCV for 5 days followed by a recovery period of 7 days. (B) Number of MSCs and in C57Bl/6 or p16-3MR mice after treatment with GCV. (C) Frequency of TMRM^{hi} MSCs in C57Bl/6 or p16-3MR mice treated with GCV. (D) p16-3MR mice were first treated with GCV as before and after the 7-day recovery period they were treated with LPS 0.5 mg/kg; they were killed at 16 hours. Flow cytometry was used to determine cell numbers of LSKs, LS-Ks, and MPPs. (E) Flow cytometry was used to measure the frequency of TMRM^{hi} LSKs, LKs, and MPPs. (F) Seahorse metabolic flux analysis was used to measure OCR in aged p16-3MR and C57Bl/6 mice after GCV treatment followed by LPS or vehicle control. Change in OCR compared with extracellular acidification rate (ECAR) is shown. (G) Changes in basal and maximal respiration. *$P < .05$, **$P < .01$ using the Mann-Whitney *U* test or two-way analysis of variance. Con, vehicle control; ns, not significant.

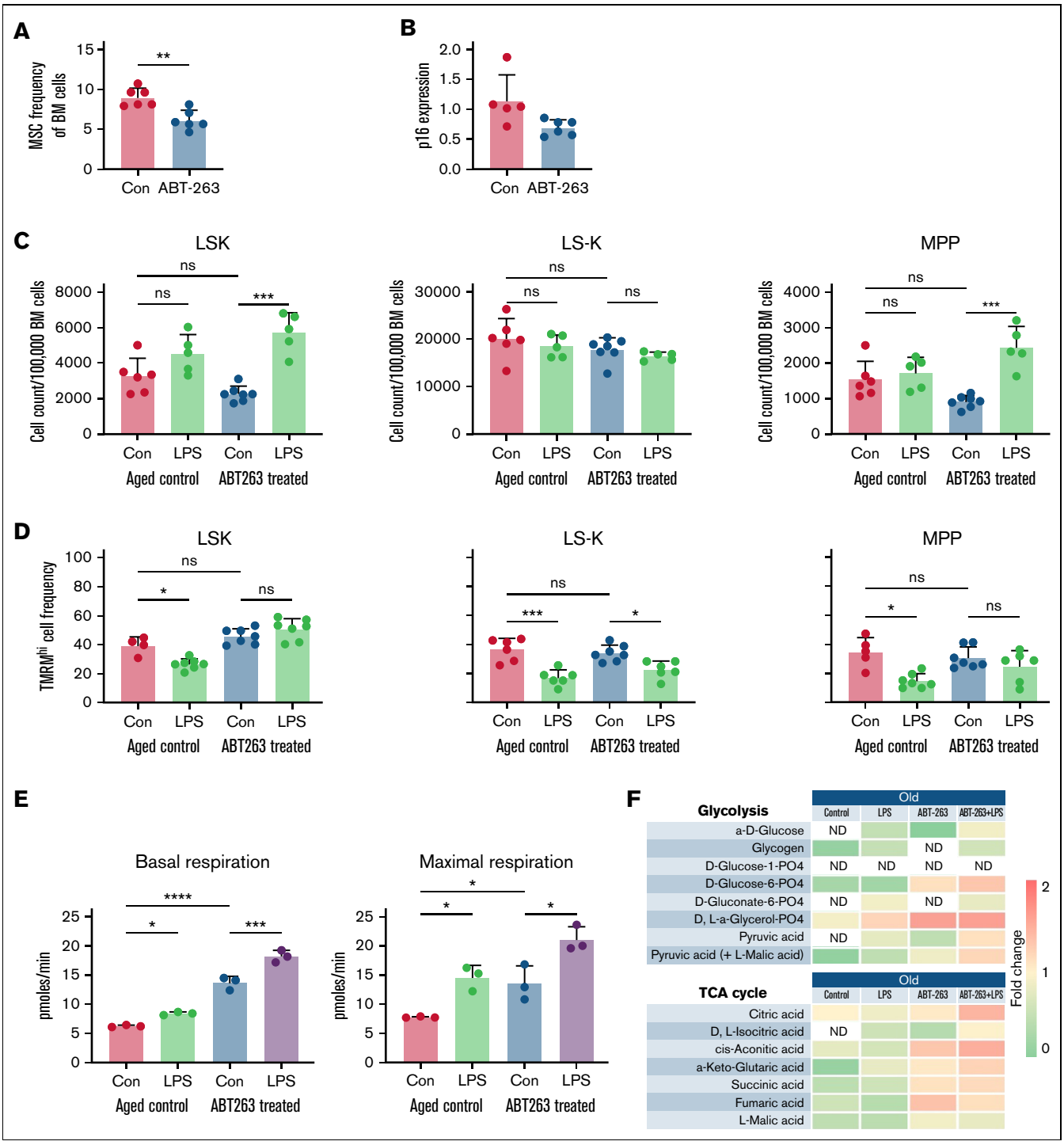

Figure 5. Treatment with the senolytic ABT-263 allows recovery of HPC mitochondrial health in aged BM. Aged C57Bl/6 mice were treated with 100 mg/kg ABT-263 or vehicle control for 7 days followed by treatment with 0.4 mg/kg LPS or vehicle control. They were killed after 12 hours and their BM isolated. (A) MSC frequency in ABT-263–treated aged mice compared with age-matched control mice. (B) MSCs were FACS-purified, and gene expression of p16 was measured by using RT-qPCR, relative to glyceraldehyde-3-phosphate dehydrogenase, in aged mice treated with ABT-263 or vehicle control. (C) Cell number of LSKs, LS-Ks, and MPPs in aged control mice and ABT-263–treated mice with or without LPS treatment. (D) Flow cytometry was used to measure the frequency of $TMRM^{hi}$ LSKs, LS-Ks, and MPPs after LPS treatment in ABT-263–treated C57Bl/6 mice and age-matched control mice. (E) Changes in basal and maximal respiration measured by Seahorse metabolic flux analysis. (F) Biolog analysis of glycolytic and TCA cycle substrates in aged mice and ABT-263–treated aged mice after LPS treatment compared with control mice. Not detected (ND) levels are labeled, and 1 represents no change. $^*P < .05$, $^{**}P < .01$, $^{***}P < .001$, $^{****}P < .0001$ using the Mann-Whitney *U* test or two-way analysis of variance. Con, vehicle control; ns, not significant.

A mechanism that has been linked to a number of age-related diseases is the accumulation of senescent cells. Cellular senescence was first described as a protective mechanism from cancer development, and the senescence-associated secretory phenotype plays an important role in tissue repair and wound healing.[14,16] However, it has become evident that with increasing age, the mechanism by which senescent cells are cleared becomes impaired,[15,29] and senescent cells accumulate in tissues and promote degenerative changes and disease development.[17-21] In this paper, we show that, similarly to other tissues, there is an accumulation of senescent cells in the BM. The senescent phenotype, characterized by the expression of $p16^{INK4A}$ and β-galactosidase staining, was not, however, observed in the HPCs residing in the BM but rather in their support cells, the MSCs. Because HPCs heavily rely on the niche and support from surrounding cells, including MSCs, it follows that accumulation of senescent cells in the BM niche can have a knock-on effect on HPC function even if they themselves do not acquire a senescent phenotype. This was demonstrated when aged HPCs were removed from the aged environment and transplanted into a young niche, where they were able to recover their function and respond more effectively to stress caused by LPS. Furthermore, it would be of interest to determine if all HPC subpopulations are able to engraft equally or whether a subset of healthier HPCs exists within the aged BM that preferentially engrafts after transplant. Although our results suggest that MSCs play a role in this recovery, it is possible that other supportive cells in the BM niche also contribute, and future work could focus on further defining the mechanism that allows the engraftment of aged HPCs in young mice and their subsequent metabolic recovery.

As the role of senescence in age-related diseases is becoming increasingly apparent, the focus has turned to developing senolytic agents that can target and potentially eliminate the senescent cell populations that accumulate with age. Our data show that the number of MSCs was increased in aged mice and that they have reduced mitochondrial function as well as overexpressed $p16^{INK4A}$ and IL-6, a component of the senescence-associated secretory phenotype. Thus, there is an accumulation of senescent MSCs in the aged BM, which could be partially driven by the decline in mitochondrial function.[11] Furthermore, we showed, using the p16-3MR mouse model, that depletion of senescent MSCs had a knock-on effect on the metabolic HPC response to stress. We were also able to show that the drug ABT-263 had a similar effect. ABT-263 is a potent inhibitor of the antiapoptotic proteins BCL-2, BCL-XL, and BCL-W, which are known to be overexpressed in senescent cells.[30] It has been shown to effectively eliminate senescent cells, and treatment with ABT-263 reportedly promotes HSC recovery after sublethal irradiation.[5] Our data suggest that ABT-263 improves HPC function indirectly through the depletion of senescent MSCs. Consequently, the remaining healthy MSCs are able to better support the HPCs in response to stress by transferring more functional mitochondria, resulting in improved mitochondrial function in the HPCs.

Many diseases, including cardiovascular disease, dementia, and cancer, increase with age and with them increases the burden on health services and society.[1,31] The impact of infections on the elderly is 2-fold: not only are older people more susceptible to infections but they are also more likely to experience more severe infections and long-term complications.[32,33] Understanding the physiological changes that occur within the aging body which lead to the susceptibility of diseases and impair the body's ability to effective respond to pathologic changes is key to improving the health span of our aging population.

In summary, we show that due to an accumulation of senescent MSCs in the aging BM niche, the MSC function to support HPCs in the rapid metabolic response to infection is impaired. By depleting senescent cells and rejuvenating the niche, it is possible to improve HPC mitochondrial health and their ability to respond to stress. This suggests that by manipulating the aging BM niche, it may be possible to improve the response to infection in the aging population.

Acknowledgments

The authors thank the Norwich Research Park, The Rosetrees Trust, The Big C, and the National Health Service. The authors also thank Allyson Tyler and Karen Ashurst from the Laboratory Medicine Department at the Norfolk and Norwich University Hospital for technical assistance. They also thank the team at the Disease Modelling Unit of the University of East Anglia for assistance with the in vivo studies.

C.H. is funded by a Wellcome Trust Clinical Research Fellowship (220534/Z/20/Z). C.H. and J.A.M. are funded by Norfolk and Norwich University Hospitals Charity Grant (51100/F049). The work was supported from the MRC project grant SAR (MR/T02934X/1). E.W. is supported by a Sir Henry Welcome Postdoctoral Fellowship (213731/Z/18/Z). J.A.M. is funded by the Rosetrees Trust (M742), A.J. is funded by the Big C (18-11R). J.G.W.S. is supported by the Academy of Medical Sciences/the Wellcome Trust/the Government Department of Business, Energy, and Industrial Strategy/the British Heart Foundation/Diabetes UK Springboard Award (SBF005\1057). N.B. is supported by the Biotechnology and Biological Sciences Research Council (BBSRC) Institute's Strategic Programme Gut Microbes and Health (BB/R012490/1: BBS/E/F/000P R10355). The author(s) acknowledge support from the Biotechnology and Biological Sciences Research Council (BBSRC), part of UK Research and Innovation, Core Capability Grant BB/CCG1720/1 and the National Capability (BBS/E/T/000P R9816).

Authorship

Contribution: C.H., K.M.B., J.G.W.S., and S.A.R. designed the research; C.H., J.A.M., J.J.M., A.J., B.B.J., and E.W. performed the research; C.H., J.J.M., N.B., and S.A.R. performed the in vivo work; J.G.W.S. and N.B. provided essential reagents and knowledge; and C.H., K.M.B., J.G.W.S., and S.A.R. wrote the paper.

Conflict-of-interest disclosure: The authors declare no competing financial interests.

ORCID profiles: E.W., 0000-0003-0531-2807; B.B.J., 0000-0002-6280-8385; K.M.B., 0000-0003-1334-4526; S.A.R., 0000-0002-3711-7558.

Correspondence: Stuart A. Rushworth and Kristian M. Bowles, Department of Molecular Haematology, Norwich Medical School, Norwich Research Park, Norwich, NR4 7UQ, United Kingdom; email: s.rushworth@uea.ac.uk and k.bowles@uea.ac.uk.

References

1. Foreman KJ, Marquez N, Dolgert A, et al. Forecasting life expectancy, years of life lost, and all-cause and cause-specific mortality for 250 causes of death: reference and alternative scenarios for 2016-40 for 195 countries and territories. *Lancet*. 2018;392(10159):2052-2090.
2. Manz MG, Boettcher S. Emergency granulopoiesis. *Nat Rev Immunol*. 2014;14(5):302-314.
3. Chambers SM, Shaw CA, Gatza C, Fisk CJ, Donehower LA, Goodell MA. Aging hematopoietic stem cells decline in function and exhibit epigenetic dysregulation. *PLoS Biol*. 2007;5(8):e201.
4. Dykstra B, Olthof S, Schreuder J, Ritsema M, de Haan G. Clonal analysis reveals multiple functional defects of aged murine hematopoietic stem cells. *J Exp Med*. 2011;208(13):2691-2703.
5. Chang J, Wang Y, Shao L, et al. Clearance of senescent cells by ABT263 rejuvenates aged hematopoietic stem cells in mice. *Nat Med*. 2016;22(1):78-83.
6. Ho TT, Warr MR, Adelman ER, et al. Autophagy maintains the metabolism and function of young and old stem cells. *Nature*. 2017;543(7644):205-210.
7. Mistry JJ, Hellmich C, Moore JA, et al. Free fatty-acid transport via CD36 drives β-oxidation-mediated hematopoietic stem cell response to infection. *Nat Commun*. 2021;12(1):7130.
8. Mistry JJ, Marlein CR, Moore JA, et al. ROS-mediated PI3K activation drives mitochondrial transfer from stromal cells to hematopoietic stem cells in response to infection. *Proc Natl Acad Sci U S A*. 2019;116(49):24610-24619.
9. Hérault A, Binnewies M, Leong S, et al. Myeloid progenitor cluster formation drives emergency and leukaemic myelopoiesis. *Nature*. 2017;544(7648):53-58.
10. Sun N, Youle RJ, Finkel T. The mitochondrial basis of aging. *Mol Cell*. 2016;61(5):654-666.
11. Wiley CD, Velarde MC, Lecot P, et al. Mitochondrial dysfunction induces senescence with a distinct secretory phenotype. *Cell Metab*. 2016;23(2):303-314.
12. Passos JF, Nelson G, Wang C, et al. Feedback between p21 and reactive oxygen production is necessary for cell senescence. *Mol Syst Biol*. 2010;6(1):347.
13. Velarde MC, Flynn JM, Day NU, Melov S, Campisi J. Mitochondrial oxidative stress caused by Sod2 deficiency promotes cellular senescence and aging phenotypes in the skin. *Aging (Albany NY)*. 2012;4(1):3-12.
14. Hayflick L. The biology of human aging. *Am J Med Sci*. 1973;265(6):432-445.
15. Campisi J. Aging, cellular senescence, and cancer. *Annu Rev Physiol*. 2013;75(1):685-705.
16. Demaria M, Ohtani N, Youssef SA, et al. An essential role for senescent cells in optimal wound healing through secretion of PDGF-AA. *Dev Cell*. 2014;31(6):722-733.
17. Abdul-Aziz AM, Sun Y, Hellmich C, et al. Acute myeloid leukemia induces protumoral p16INK4a-driven senescence in the bone marrow microenvironment. *Blood*. 2019;133(5):446-456.
18. Saez-Atienzar S, Masliah E. Cellular senescence and Alzheimer disease: the egg and the chicken scenario [published correction appears in *Nat Rev Neurosci*. 2020;21(10);587]. *Nat Rev Neurosci*. 2020;21(8):433-444.
19. Chinta SJ, Woods G, Demaria M, et al. Cellular senescence is induced by the environmental neurotoxin paraquat and contributes to neuropathology linked to Parkinson's disease. *Cell Rep*. 2018;22(4):930-940.
20. Jeon OH, David N, Campisi J, Elisseeff JH. Senescent cells and osteoarthritis: a painful connection. *J Clin Invest*. 2018;128(4):1229-1237.
21. Childs BG, Baker DJ, Wijshake T, Conover CA, Campisi J, van Deursen JM. Senescent intimal foam cells are deleterious at all stages of atherosclerosis. *Science*. 2016;354(6311):472-477.
22. Geiger H, de Haan G, Florian MC. The ageing haematopoietic stem cell compartment. *Nat Rev Immunol*. 2013;13(5):376-389.
23. Beerman I, Maloney WJ, Weissmann IL, Rossi DJ. Stem cells and the aging hematopoietic system. *Curr Opin Immunol*. 2010;22(4):500-506.
24. Mansell E, Sigurdsson V, Deltcheva E, et al. Mitochondrial potentiation ameliorates age-related heterogeneity in hematopoietic stem cell function. *Cell Stem Cell*. 2021;28(2):241-256.e6.
25. Koide Y, Morikawa S, Mabuchi Y, et al. Two distinct stem cell lineages in murine bone marrow. *Stem Cells*. 2007;25(5):1213-1221.
26. Worthley DL, Churchill M, Compton JT, et al. Gremlin 1 identifies a skeletal stem cell with bone, cartilage, and reticular stromal potential. *Cell*. 2015;160(1-2):269-284.
27. Sharpless NE, Sherr CJ. Forging a signature of in vivo senescence [published correction appears in *Nat Rev Cancer*. 2015;15(8):509]. *Nat Rev Cancer*. 2015;15(7):397-408.
28. Muñoz-Espín D, Serrano M. Cellular senescence: from physiology to pathology. *Nat Rev Mol Cell Biol*. 2014;15(7):482-496.

29. Hall BM, Balan V, Gleiberman AS, et al. Aging of mice is associated with p16(Ink4a)- and β-galactosidase-positive macrophage accumulation that can be induced in young mice by senescent cells. *Aging (Albany NY)*. 2016;8(7):1294-1315.
30. Yosef R, Pilpel N, Tokarsky-Amiel R, et al. Directed elimination of senescent cells by inhibition of BCL-W and BCL-XL. *Nat Commun*. 2016;7(1):11190.
31. Partridge L, Deelen J, Slagboom PE. Facing up to the global challenges of ageing. *Nature*. 2018;561(7721):45-56.
32. Yoshikawa TT. Epidemiology and unique aspects of aging and infectious diseases. *Clin Infect Dis*. 2000;30(6):931-933.
33. Gavazzi G, Krause KH. Ageing and infection. *Lancet Infect Dis*. 2002;2(11):659-666.